Decarboxylation involving a ferryl, propionate, and a tyrosyl group in a radical relay yields heme *b*

Received for publication, November 7, 2017, and in revised form, February 1, 2018 Published, Papers in Press, February 2, 2018, DOI 10.1074/jbc.RA117.000830

Bennett R. Streit[‡], Arianna I. Celis[‡], Garrett C. Moraski[‡], Krista A. Shisler[‡], Eric M. Shepard[‡], Kenton R. Rodgers[§], Gudrun S. Lukat-Rodgers[§], and Jennifer L. DuBois[‡1]

From the [‡]Department of Chemistry and Biochemistry, Montana State University, Bozeman, Montana 59717-3400 and the [§]Department of Chemistry and Biochemistry, North Dakota State University, Fargo, North Dakota 58108-6050

Edited by F. Peter Guengerich

The H_2O_2-dependent oxidative decarboxylation of coproheme III is the final step in the biosynthesis of heme *b* in many microbes. However, the coproheme decarboxylase reaction mechanism is unclear. The structure of the decarboxylase in complex with coproheme III suggested that the substrate iron, reactive propionates, and an active-site tyrosine convey a net $2e^-/2H^+$ from each propionate to an activated form of H_2O_2. Time-resolved EPR spectroscopy revealed that Tyr-145 formed a radical species within 30 s of the reaction of the enzyme–coproheme complex with H_2O_2. This radical disappeared over the next 270 s, consistent with a catalytic intermediate. Use of the harderoheme III intermediate as substrate or substitutions of redox-active side chains (W198F, W157F, or Y113S) did not strongly affect the appearance or intensity of the radical spectrum measured 30 s after initiating the reaction with H_2O_2, nor did it change the ~270 s required for the radical signal to recede to ≤10% of its initial intensity. These results suggested Tyr-145 as the site of a catalytic radical involved in decarboxylating both propionates. Tyr-145$^\bullet$ was accompanied by partial loss of the initially present Fe(III) EPR signal intensity, consistent with the possible formation of Fe(IV)=O. Site-specifically deuterated coproheme gave rise to a kinetic isotope effect of ~2 on the decarboxylation rate constant, indicating that cleavage of the propionate Cβ–H bond was partly rate-limiting. The inferred mechanism requires two consecutive hydrogen atom transfers, first from Tyr-145 to the substrate Fe/H_2O_2 intermediate and then from the propionate Cβ–H to Tyr-145$^\bullet$.

Metallotetrapyrroles are among nature's oldest and most versatile catalytic scaffolds. Their functional versatility is due to the macrocycle's capacity for accommodating a variety of metals at the center and organic functional groups around the periphery. Many well-characterized enzymes that use a metallotetrapyrrole as a substrate, such as heme oxygenase (1, 2), heme A synthase (3), or some cytochrome P450s (4), take advantage of its intrinsic reactivity, so that these reactions have an autocatalytic character. Coproheme decarboxylase is a metallotetrapyrrole-modifying enzyme that likewise uses a heme as both substrate and cofactor, catalyzing the oxidative decarboxylation of ferric 2,4,6,7-tetrapropionic acid porphyrin (coproheme) to yield ferric 6,7-dipropionic acid-2,4-divinyl porphyrin (heme *b*). This reaction is the final step in the heme biosynthetic pathways of diverse Gram-positive bacteria and possibly some Archaea (5), encoded by a gene alternately referred to as *cld* or *hemQ* or, most recently, as *chdC* (5, 6).

Each decarboxylation is an oxidation in which a net two electrons and two protons are transferred from the reactive propionate to a molecule of H_2O_2, yielding $2H_2O$, CO_2, and a new vinyl group (7, 8). H_2O_2 activation at the open coordination position on the substrate iron (distal pocket) could generate any of a number of well-known reactive species, including a ferric hydroperoxy (Fe(III)–OOH), ferryl porphyrin π-cation radical (Fe(IV)=O (por$^{+\bullet}$), compound I), or ferryl complex (Fe(IV)=O or Fe(IV)–OH, compound II). The structure of the decarboxylase bound to coproheme (9), however, showed that the reactive propionates are positioned pointing away from the distal pocket; their orientation below the porphyrin plane prohibits any direct access of the reactive propionates to an Fe/H_2O_2 species (Fig. 1). This suggested a more complicated reaction mechanism where, like in heme side chain–modifying enzymes (3, 4) or cyclooxygenases (10), electrons or protons might be conveyed from the substrate to a reactive iron intermediate via a redox-active amino acid side chain. Such transfers of protons and electrons could occur sequentially or by proton-coupled electron transfer. Alternatively, homolytic scission of an Fe(III)coproheme–OOH bond could yield a hydroxyl radical ($^\bullet$OH) that is channeled by the active site toward a specific C–H bond on the reactive propionate. A mechanism of this type would be consistent with the proposed self-hydroxylation catalyzed by heme oxygenases (1) and with the decarboxylase structure (9), which lacks the typical apparatus of enzymes that activate H_2O_2 by heterolytic cleavage. How the enzyme would convey a highly reactive $^\bullet$OH to specific sites of reaction on the two propionates is unclear.

To distinguish among these pathways, EPR spectroscopy and kinetic methods were used to monitor the coproheme decarboxylation using WT, mutant, and site-selectively deuterated proteins as well as deuterium-labeled substrates. Strong experimental evidence is presented in support of a mechanism where the substrate iron activates H_2O_2, Tyr-145 forms a radical spe-

This work was supported by NIGMS, National Institutes of Health, Grants R01GM090260 (to J. L. D.) and R15GM114787 (to G. S. L.-R.). The authors declare that they have no conflicts of interest with the contents of this article. The content is solely the responsibility of the authors and does not necessarily represent the official views of the National Institutes of Health.

This article contains Table S1 and Figs. S1–S5.

[1] To whom correspondence should be addressed: Dept. of Chemistry and Biochemistry, Montana State University, Bozeman, MT 59715. Tel.: 406-994-2844; E-mail: jennifer.dubois1@montana.edu.

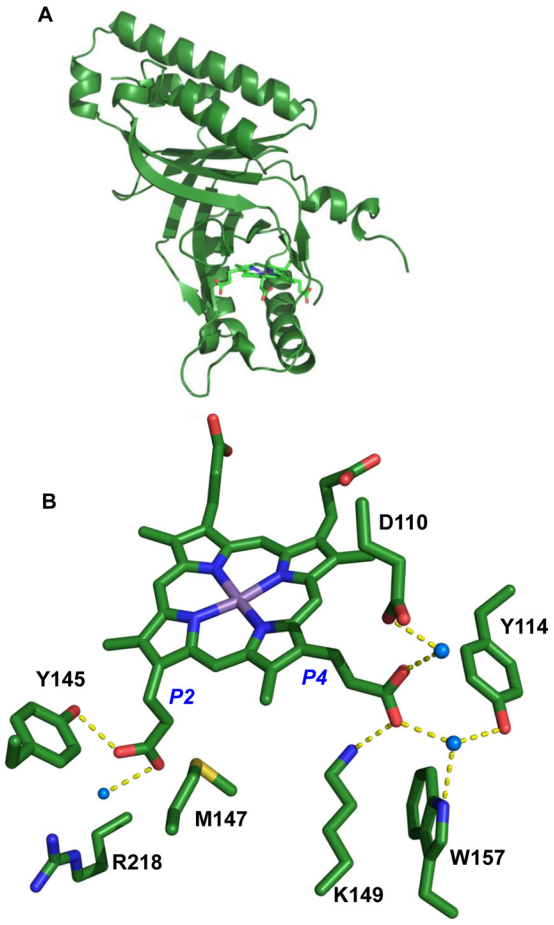

Figure 1. Coproheme decarboxylase subunit and active site structure with the substrate analog, manganese coproporphyrin, bound (PDB ID: 5T2K). *A*, the subunit structure of coproheme decarboxylase (*green schematic*) showing a bound manganese coproheme. The unreactive pair of propionates points toward the solvent exterior and to the *right* in this diagram. *B*, residues hydrogen-bonded to reactive propionates 2 (*P2*) and 4 (*P4*) are indicated with *dashed lines*. Tyr-145, Tyr-113, Trp-157, and Trp-159 are all redox-active side chains and potential sites of catalytic radical formation. Trp-159, in the foreground of P4 in this view, has been omitted for clarity. Three water molecules involved in hydrogen-bonding networks to each propionate are included. Atoms are labeled: carbon (*green*), nitrogen (*blue*), oxygen (*red*), and iron (*purple*).

cies via hydrogen atom transfer, and the resulting Tyr-145 radical (Tyr-145$^{\bullet}$) acts as the unique intermediary for hydrogen atom transfer from both reactive propionates.

Results

Deuterium-labeled coproheme III was generated in high yield

Deuterium-labeled coproporphyrinogen III (Fig. S1) was prepared in a single step by co-incubating 3,3,5,5-$^2H_4$-aminolevulinic acid (D_4-ALA)[2] and the enzymes HemB–E in buffer in an anaerobic chamber. Colorless D-coproporphyrinogen III was subsequently oxidized to pink D-coproporphyrin III using HemY and O_2 from ambient air. The HPLC trace for the HemBCDEY reaction (Fig. S1) confirms that the product has a retention time matching a pure coproporphyrin III standard, with minimal detectable contaminants with absorbance in the 300–700-nm range. The predicted exact mass for the $[M + H]^+$ ion (667.3 g/mol, M = $C_{36}H_{26}D_{12}N_4O_8$) is observed in the mass spectrum (Fig. S1), with the same expected isotopic distribution reported previously for D-coproporphyrin (MS, $[M + H]^+$: 667.3 Da, determined distribution: M_{full}, 1.4%; M_{full}-*1D*, 5.2%; M_{full}-*2D*, 15.8%; M_{full}-*3D*, 20.2%; M_{full}-*4D*, 20.9%; M_{full}-*5D*, 19.5%; M_{full}-*6D*, 11%; M_{full}-*7D*, 4.6%; M_{full}-*8D*, 1.3%; M_{full}-*9D*, 0.2%). The starting materials and products were subsequently analyzed by ^{1}H NMR (Fig. S2). The data show loss of intensity in peaks associated with the four propionate β-carbons (4.55 ppm) and the four tetrapyrrole-bridging *meso* carbons (11.2–11.3 ppm), indicating that the protons at these positions have been substituted with deuterium. Consistent with prior work (11), substitution at the *meso* positions is not complete, suggesting that a small amount of reintroduction of ^{1}H occurs during the biosynthesis. The molar yield of pure D-coproporphyrin III, based on the amount of D_4-ALA used in the reaction, was 90 ± 5% of the expected theoretical yield.

D-Tyr-labeled decarboxylase was generated in low yield and its reaction was less efficient than that of unlabeled protein

Typical pure protein yields for the decarboxylase were ~8 mg/liter culture. By contrast, pure D-Tyr-labeled enzyme was produced at 2 mg/liter culture, due to low levels of expression in the Tyr auxotrophic strain. Complete conversion of substrate to product required 400 eq of H_2O_2 (pH 7.4 potassium phosphate, 20 °C). Under those conditions, the reaction was complete within 1 min (Fig. S3).

By contrast, prior work showed that ~10 eq of H_2O_2 was sufficient to convert the WT/unlabeled enzyme–coproheme complex to heme *b*; the small excess of H_2O_2 was required due to competing side reactions between H_2O_2 and the protein/heme (7, 9). A ferric harderoheme complex accrues with a formation rate constant previously fitted to $k = 2.9\ min^{-1}$ or $t_{½}$ = 14 s, and heme *b* forms with $k = 0.30\ min^{-1}$ ($t_{½}$ = 140 s, pH 7.4 potassium phosphate, 20 °C) (7).

Time-resolved EPR demonstrated formation and decay of an organic radical reaction intermediate

The decarboxylase–coproheme complex and 10 eq of H_2O_2 were manually mixed (pH 8.8, 20 °C) and subsequently freeze-trapped in EPR tubes at time points from 0.5 to 5 min. The resulting 77 K, X-band EPR spectra illustrated the formation of an EPR-active S = ½ species within 0.5 min that subsequently decayed nearly to baseline over the next 5 min (Fig. 2*A*). Although a full EPR kinetic time course is lacking, the appearance of the S = ½ species within 0.5 min of mixing and its subsequent decay within 300 s are kinetically consistent with its assignment as an intermediate in the conversion of coproheme to heme *b*, based on the expected reaction $t_{½}$ = 140 s for heme *b* formation cited above (7). Moreover, the 14-s half-life for the initial decarboxylation of P2 to yield harderoheme and the ~300-s lifetime of the radical species overall suggest that the observed EPR signals most likely represent superimposed radical intermediate density from both the decarboxylations of P2 and P4, particularly at the later time points (7). This observation is consistent with prior stopped-flow analyses, which showed

[2] The abbreviations used are: D_4-ALA, 3,3,5,5-$^2H_4$-aminolevulinic acid; μW, microwatt(s); mW, milliwatt(s).

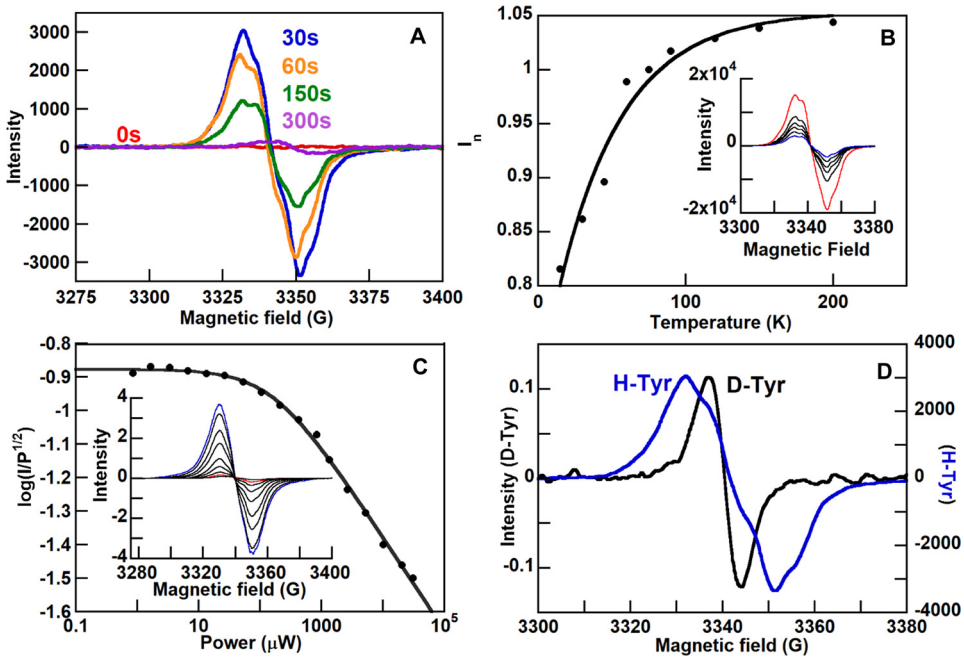

Figure 2. Properties of the side chain radical intermediate generated along the pathway to coproheme decarboxylation. *A*, a radical forms within 30 s of mixing 100 μM decarboxylase–coproheme complex with 10 eq of H_2O_2 and then decays to baseline over time. Spectra were measured for samples frozen at the indicated time points at 26 μW, 77 K, pH 8.8. Spin quantitation of the 30-s sample spectrum relative to a TEMPO standard curve indicated a 35 μM concentration of the radical species. *B*, the effect of temperature on normalized EPR signal intensity (Equation 2) was measured for the 30-s sample from 15 to 200 K (*A*). An extrapolated curve illustrates the trend in the data points. *Inset*, full spectra measured at 30 (*red curve*), 60, 90, 120, 150, and 200 (*blue curve*) K are shown, illustrating the isotropic diminution of the signal with decreasing temperature. *C*, the power saturation behavior for the 30-s sample in *A* was determined from 0.85 μW to 39 mW. The data were fit to Equation 3, yielding $P_{1/2} = 190 \pm 30$ μW. *Inset*, full spectra are shown for every other point on the plot, from 1.7 μW (*red curve*) to 39 mW (*blue curve*), illustrating the isotropic loss of signal with increasing power. *D*, the EPR spectrum measured for the sample frozen at 30 s in *A* is overlaid with a sample prepared in a similar manner but with protein in which all of the tyrosine side chains were fully deuterated. Upon deuteration, the peak-to-trough line width narrows from 20 to 7 G, and the fine structure is lost, consistent with the radical's assignment as a tyrosyl.

that the P2 and P4 decarboxylations were similar in rate and not temporally well-resolved (8).

Double integration of the 0.5-min sample spectrum and comparison with a TEMPO standard curve indicated that it contained a 35 μM concentration of the EPR-active species per 100 μM decarboxylase–coproheme complex initially present, where the complex converts nearly stoichiometrically to decarboxylase–heme *b* under the conditions used. The spectrum showed a partially resolved four-line signal centered at g = 2.005 with a peak-to-trough line width of ~20 G (Fig. S4), consistent with an amino acid side chain radical (see below) (12).

The organic radical is localized on a tyrosine side chain

To gain more information about the radical species, spectra for the 0.5-min sample were measured as a function of applied microwave power and at varying temperatures (Fig. 2, *B* and *C*). Increasing power yielded a series of similar looking traces that diminished in intensity with $P_{1/2} = 190$ μW. A value in this range is consistent with an amino acid–based radical that is not strongly exchange-coupled to the electronic spin of a nearby paramagnetic metal. Coupling would enhance the spin-lattice relaxation for the radical and raise $P_{1/2}$. Values of $P_{1/2}$ for compound I, for example, where the por$^{\bullet+}$ radical is strongly exchange-coupled to the heme Fe(IV) ($S = 1/2$) are typically >5 mW (13–15). For heme proteins in which the por$^{\bullet}$+ from compound I migrates to a nearby but still Fe(IV) exchange–coupled tyrosine (*e.g.* cytochrome P450 cam), $P_{1/2}$ = 1 mW (16). The effect of temperature on the spectrum was likewise characteristic of an organic side-chain radical (17), with signal intensity diminishing steadily as the temperature was lowered from 200 to 30 K. The isotropic diminution in spectral intensity with either increasing power or decreasing temperature is suggestive of a single organic radical rather than a distribution of species.

To test whether the radical species was a tyrosyl, the protein was expressed with all of its tyrosine side chains carbon-deuterated. The deuterium nucleus has an integer spin ($I_D = 1$) that couples weakly to the electron spin relative to the protium nucleus ($I_H = 1/2$); perdeuteration consequently eliminates the doublet hyperfine splitting observed for ^{1}H in the EPR spectra of tyrosyl radicals. Moreover, deuteration narrows the EPR peak-to-trough line width for free tyrosine from 21 to 8 G (12). Consistent with its assignment as a neutral tyrosyl radical, the spectrum measured for the Tyr-deuterated decarboxylase following reaction with 400 eq of H_2O_2 (<30 s) displayed no hyperfine features and a significantly narrowed line width (7 G) (Fig. 2*D*).

The EPR spectrum for the intermediate can be simulated with hyperfine coupling due to the Tyr-145 methylene protons and slight g-anisotropy

Studies of site-specifically deuterated tyrosines have shown that the electron spin of the tyrosyl radical localizes on the ring 1, 3, and 5 carbons (12, 18). Coupling of the electron spin to ^{1}H on carbons 3 and 5 is weak and relatively insensitive to the protein environment. Doublet splitting due to each of the two methylene Cβ protons (H_A and H_B; Scheme 1), however, con-

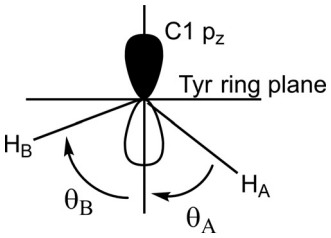

SCHEME 1. Doublet splitting.

stitutes the major contributor to hyperfine structure and depends on each proton's position relative to the p_z orbital on the ring C1, according to Equation 1,

$$A_H = B_0\rho + B_1\rho\cos^2\theta \qquad \text{(Eq. 1)}$$

where A_H is the isotropic hyperfine coupling due to Cβ-H for H_A or H_B, ρ is the ring carbon unpaired electron spin density (ranging over 0.35–0.42 for C1 for known protein tyrosyl radicals), and B_1 is a constant (58 G for tyrosyl radicals) (12, 18, 19). $B_0 \ll B_1$ and is usually neglected (12).

Analysis of the crystal structure for the homopentameric decarboxylase–coproheme complex (Protein Data Bank (PDB) code 5T2K) (9) allowed us to identify an average $\Theta_A = 45.41 \pm 2.20°$ and $\Theta_B = 72.21 \pm 2.01°$ for Tyr-145 (errors represent ±1 S.D.). Inserting each of these angles and $\rho = 0.35–0.42$ into Equation 1 yielded predicted hyperfine coupling constants $A_{HA} = 10–12$ G and $A_{HB} = 1.9–2.3$ G. These ranges and g = 2.005 gave starting values for fitting the spectrum for the intermediate trapped at 30 s (Fig. S4). The fit refined to give $A_{HA} = 9.6$ and $A_{HB} = 2.5$ G, each of which is close to the predicted range. A small degree of g-anisotropy ($g_1 = 2.006, g_2 = 2.005, g_3 = 2.004$) improved the fit, possibly reflecting small differences in the individual subunits of the homopentamer or delocalization of radical character onto other tyrosines (total of 9 per monomer). Hence, the spectrum appears to be consistent with a radical on residue Tyr-145. Accurate simulation of the X-band EPR spectrum, without making assumptions about the identity or structure of the tyrosine giving rise to the spectrum, the likely degree of g-anisotropy, or the range of values for ρ, will require further analysis of the corresponding high-field EPR spectrum, using g_x to solve for θ and ρ, as described previously (19).

Loss of the EPR radical signal specifically in the Y145S mutant suggests that Tyr-145 is the site of the radical intermediate

Four aromatic amino acids that could potentially harbor radical electron density (20) surround the pair of reactive propionates: Tyr-145 (propionate 2) and Trp-198, Trp-157, and Tyr-113 (propionate 4) (Fig. 1). Substitution of each of the latter three by redox-inactive residues had little or no effect on the number of H_2O_2 equivalents required to convert the enzyme–coproheme complex to heme *b*, although there were some differences in HPLC profiles of porphyrin-containing products *versus* [H_2O_2]. The W198F mutant, for example, accumulated relatively more harderoheme intermediate than WT, whereas the heme *b* product bound to Y113S was more susceptible to H_2O_2-mediated degradation. These differences suggested that Tyr-113, Trp-198, and Trp-157 may play some role in the coproheme/heme *b* conversion, but not as an essential catalytic component.

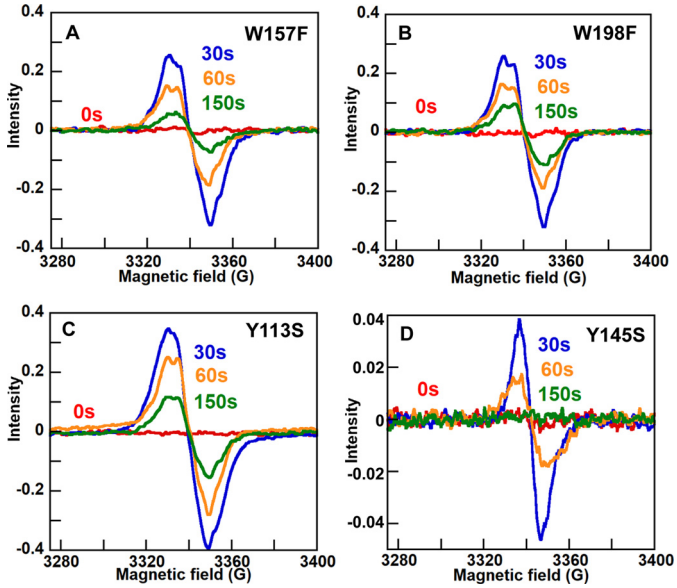

Figure 3. The side-chain radical intermediate formed in W157F, W198F, and Y113S decarboxylase mutants has similar properties to WT decarboxylase, whereas Y145S is distinct. 100 μM coproheme complexes of the W157F (*A*), W198F (*B*), Y113S (*C*), and Y145S (*D*) decarboxylase mutants were rapidly mixed with 10 eq of H_2O_2 and subsequently frozen at the indicated time points. EPR spectra measured for the first three mutants resemble one another, and the 30-s sample was measured for the WT enzyme (Fig. 2). By contrast, the Y145S sample had a narrower line width and distinct g-values (see Fig. S3, Table S1, and "Results"). Spin quantitation of the spectra measured for the 30-s samples indicated that 30 (*A*), 30 (*B*), 42 (*C*), and 3.8 μM (*D*) concentrations of the radical species had formed (compare with WT in Fig. 2*A*, where 35 μM accumulated). The radical species formed in the Y145S sample was not apparent above baseline by 150 s.

The Y145S mutant, by contrast, exhibited no decarboxylase activity, regardless of the amount of H_2O_2 added (9). Instead, after the addition of 3000 eq of H_2O_2, 90% of the initially present coproheme had degraded to a product without an observable UV-visible chromophore. These experiments suggested that Tyr-145 was possibly the site of a catalytic radical.

To test this hypothesis and to determine whether the radical formed in a localized manner, coproheme complexes of the W198F, W157F, Y113S, and Y145S mutants were examined for their ability to form radicals during turnover with H_2O_2. Following reaction with 10 eq of H_2O_2, the W198F, W157F, and Y113S mutants formed radical species with EPR spectral features that were highly similar to each other and to WT (Fig. S4). Small discrepancies in the fitted g-values and hyperfine coupling constants suggest that the radical is sensitive to the changes in the chemical environment that these mutations produce (Table S1). Spin quantitation of the spectrum measured for the 30-s samples indicated 30, 30, and 42 μM concentrations of the radical species had formed in the W198F, W157F, and Y113S mutants (S.D. values for three measurements were ≤10% of the measured intensity). For comparison, the WT decarboxylase accumulated a 35 μM concentration of the radical species at 30 s. In each case, the radical species diminished in intensity over time, reaching ≤25% of the integrated intensity at 30 s by 150 s (Fig. 3, *A–C*) and receding to baseline within 300 s.

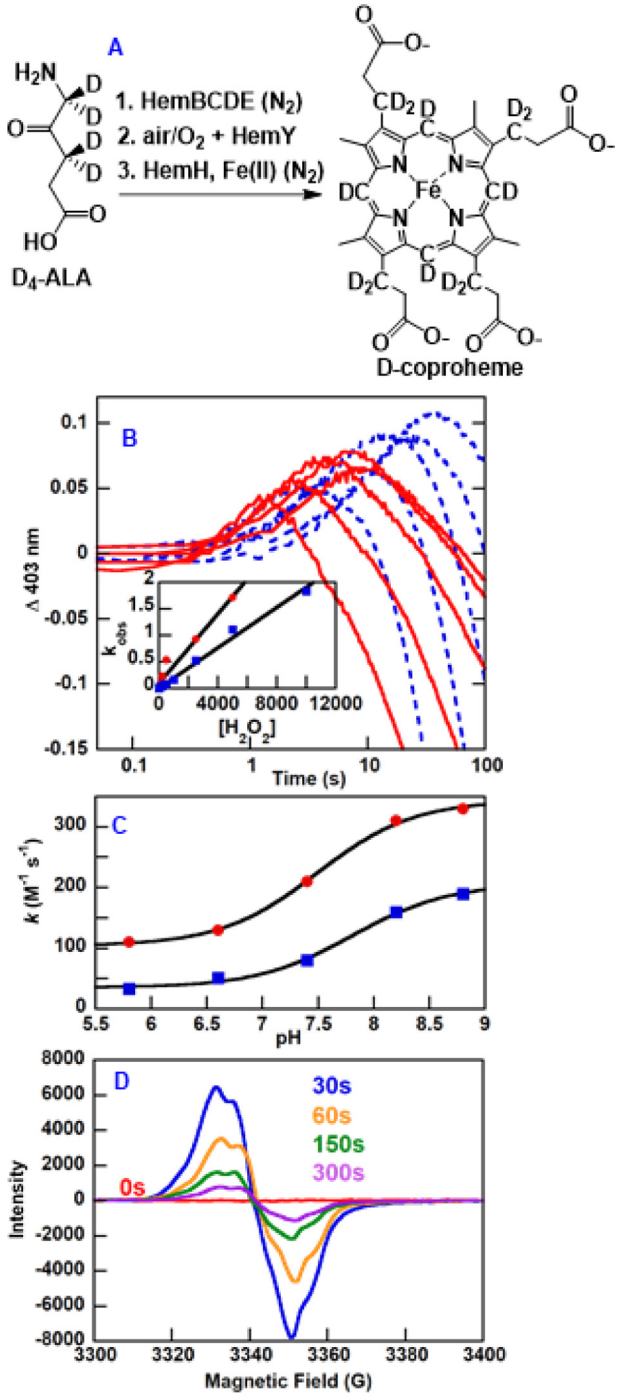

Figure 4. The decarboxylation of CβD$_2$-coproheme is ~2-fold slower than CβH$_2$-coproheme and results in substantially greater accumulation of Tyr-145$^\bullet$. *A*, summary of the biosynthetic scheme for CβD$_2$-coproheme from D$_4$-ALA, illustrating the expected positions of deuterium label incorporation. *B*, reactions of 10 μM decarboxylase–coproheme (*red lines*) or –CβD$_2$-coproheme (*blue dashes*) with 15, 25, 50, 100, or 250 eq of H_2O_2 (increasing concentrations, *right* to *left*) were monitored over time via stopped-flow UV-visible spectroscopy (50 mM potassium phosphate, pH 7.4, 25 °C). The traces measured at 402 nm (shown) were fit to two the sum of two exponentials. The first phase corresponded to the formation of the decarboxylase–heme *b* complex and the second to heme *b* decay (8). *Inset*, k_{obs} values derived from fits to the initial phase are plotted *versus* [H_2O_2]. Linear fits to the data yielded second-order rate constants 210 and 80 M^{-1} s^{-1} for coproheme (*red circles*) and CβD$_2$-coproheme (*blue squares*), respectively. *C*, second-order rate constants for the reactions described in *A* were measured as a function of pH and were fit to the same pK_a. *D*, the tyrosyl radical formed during a single turnover of the decarboxylase–D-coproheme complex (100 μM + 10 eq of H_2O_2) was monitored at 30 s, along with its subsequent decay. Spectra were measured at 0.026 mW, 77 K, pH 8.8. Spin quantitation of the spectrum measured for the 30-s sample indicated 75 μM of the radical species had formed.

By contrast, the Y145S–coproheme complex formed no appreciable radical species under the same reaction conditions. Following the addition of a large excess of H_2O_2 (300 eq), a small amount of an EPR-observable $S = ½$ species formed (3.8 μM/100 μM protein) (Fig. 3*D*). The peak-to-trough line width (11 G) was narrower than the spectra in Fig. 2*A* or Fig. 3 (*A*–*C*), the spectrum decayed to baseline more rapidly following the addition of H_2O_2 (within 150 s), and the spectrum measured at 30 s lacked any detectable hyperfine splitting (Fig. S5 and Table S1). Whereas the identity/nature of the radical in this mutant is currently unresolved, it is clear that this species is off the reaction pathway. The dependence of product formation on Tyr-145, the formation of an $S = ½$ radical whose microwave power and temperature dependences are consistent with an organic radical, and the temporal correlation of the radical decay with product formation support the conclusion that Tyr-145 is the site of a mechanistically crucial radical-based intermediate.

Cleavage of the 2-propionate Cβ–H bond by the Tyr-145 radical is partly rate-limiting

Tyr-145$^\bullet$ is well-positioned to remove a hydrogen atom from the coproheme propionate 2 on the carbon β to the tetrapyrrole (Fig. 1) (9). A substrate radical at this position would be conjugated to and resonance-stabilized by the macrocycle. To test whether C–H bond cleavage occurs at this position, coproheme with deuterium substituted for protium at all of its propionate β-carbons was prepared. Its reaction with H_2O_2 was studied over time via stopped-flow UV-visible and freeze-quench EPR spectroscopies. The reaction exhibited biphasic kinetics in which the first phase was linearly dependent on H_2O_2 concentration and led to heme *b* formation (Fig. 4*A*). The second phase was independent of H_2O_2 and led to loss of the heme *b* chromophore. Second-order rate constants determined for the first phase as a function of pH are plotted in Fig. 4*B* along with data previously measured for unlabeled coproheme (8). The rate constants in each case had identical although modest (~3-fold) pH dependences, with a pK_a = 7.4 and a k_D/k_H kinetic isotope effect of ~2 across the entire pH range. We conclude that the Cβ–H bond is cleaved during the decarboxylation reaction; because the theoretically expected value for a primary hydrogen/deuterium kinetic isotope effect is 7 (21, 22), this step probably only partially limits the rate of coproheme/heme *b* conversion. The D-coproheme/H_2O_2 reaction was subsequently monitored over time by freeze-quench EPR (Fig. 4*C*). The amount of Tyr-145$^\bullet$ accumulating at 0.5 min dramatically increased, relative to the unlabeled substrate, to 75 μM/100 μM protein. The Tyr-145$^\bullet$ signal likewise took longer (>30 min instead of ~5 min) to return to baseline for the deuterated complex (data shown to 300 s). These results collectively suggest that Tyr-145$^\bullet$ forms immediately before, and is responsible for, cleavage of the Cβ–D bond.

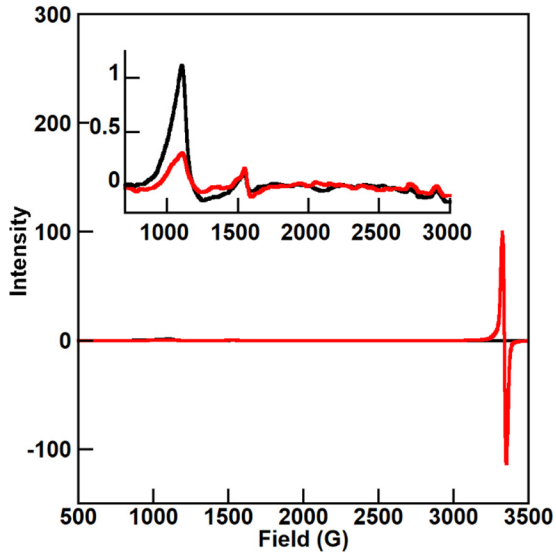

Figure 5. Time-resolved EPR spectra show a ferric $S = 5/2$ component that diminishes in intensity as the $S = 1/2$ signal due to Tyr-145• forms. The X-band EPR spectrum of the decarboxylase–CβD$_2$-coproheme complex (shown at 77 K in Fig. 3*C*) was remeasured at low temperature (15 K) and over a broad magnetic field to visualize the substrate-bound iron at $t = 0$ (*black lines*, 100 μM, 0.850 mW, pH 8.8). The 15 K spectrum for the sample measured 30 s after the addition of 10 eq of H_2O_2 is shown in *red*. The 700–3000-G region is shown at an *amplified scale* in the *inset*. An $S = 5/2$ signal, attributed to the ferric CβD$_2$-coproheme, is apparent at both time points, diminishing in intensity from 97 $\pm$ 5 μM at 0 s to 25 $\pm$ 5 μM at 30 s. Over the same time interval, the $S = 1/2$ signal attributed to Tyr-145• in Fig. 4*C* formed (75 $\pm$ 5 μM).

Tyr-145• formation is accompanied by loss of the high-spin iron signal

EPR spectra were remeasured at 15 K for the $t = 0$ and 30 s samples from Fig. 4*C* to characterize changes at the iron center that accompany formation of Tyr-145• (Fig. 5). The spectrum measured at 0 s was largely high-spin ($S = 5/2$) and rhombic, similar to spectra previously reported for HemQ-coproheme complexes from *Staphylococcus aureus* and *Listeria monocytogenes* (23). At 30 s, no obvious new signals due to iron species appeared. Instead, ~70% of the doubly integrated spectral intensity was lost from the $t = 0$ s high-spin signal. At the same time, the $S = 1/2$ signal attributed to Tyr-145• appeared (77 K data shown in Fig. 2). These data are consistent with the conversion of some of the initially available Fe(III) to an EPR-silent iron species, such as low-spin Fe(IV)=O ($S = 0$), as Tyr-145• forms.

Tyr-145• also catalyzes the decarboxylation of the ferric harderoheme intermediate

The data presented above suggest that Tyr-145• facilitates the initial, slower decarboxylation of coproheme to harderoheme. Data presented here and previously also suggest that, if a similar radical mechanism is used for conversion of harderoheme to heme *b*, Tyr-145 is also responsible. Specifically, reactions of the W198F, W157F, and Y113S mutants were not interrupted at the harderoheme/heme *b* interconversion step, and the Y145S mutant did not yield heme *b* (7). To examine directly whether Tyr-145• is also involved in the harderoheme/heme *b* conversion, the decarboxylase–harderoheme complex was generated, and its reaction with 10 eq of H_2O_2 was followed over time by freeze-quench EPR. A radical species with features

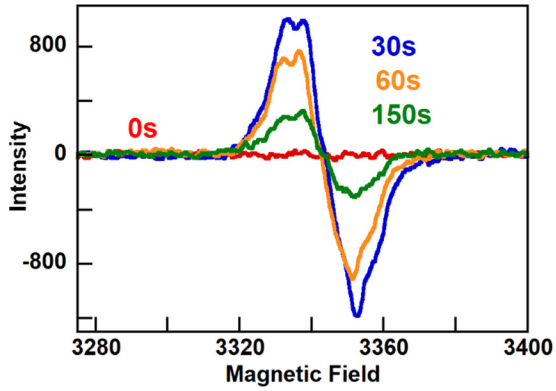

Figure 6. The ferric decarboxylase–harderoheme complex is also decarboxylated via a Tyr-145 radical. Tyrosyl radical and its decay were monitored during a single turnover of the decarboxylase–harderoheme complex (100 μM + 10 eq of H_2O_2). Spectra were measured at 0.026 mW, 77 K, pH 8.8. Spin quantitation of the spectrum measured for the 30-s sample indicated that a 12 μM concentration of the radical species had formed. The EPR spectrum for the intermediate ($g_{1,2,3}$ = 2.008, 2.005, 2.000) and the time required for its decay are similar to those measured for the radical involved in the decarboxylase–coproheme reaction (Fig. 2 and Table S1), suggesting that Tyr-145 is also involved in decarboxylating propionate 4.

similar to those in Fig. 2 formed and decayed over time (Fig. 6, Fig. S4, and Table S1). Product analysis identified the end species of the reaction as heme *b* (7). These data suggest that Tyr-145• forms and reacts in the harderoheme-bound enzyme and may therefore also be responsible for decarboxylating propionate 4.

Discussion

Heme biosynthesis in many bacteria concludes with a pair of oxidative decarboxylations. Coproheme serves as both substrate and cofactor in these reactions, and the two vinyl groups of heme *b* are products. A similar heme- and H_2O_2-dependent reaction is catalyzed by the unusual cytochrome P450, OleT. This enzyme reacts with H_2O_2 to form the catalytic Fe(IV)=O (por$^{+\bullet}$) species, which in turn directly abstracts a hydrogen atom from the carbon at the β-position relative to the carboxylate group of a fatty acid. For long-chain substrates (C_n, $n \geq 20$), this is followed by transfer of an electron and proton to the resulting Fe(IV)–OH (por), yielding Fe(III)por, CO_2, the n-1 alkene, and water (24).

Although coproheme decarboxylase catalyzes a similar reaction, its structural constraints are different from those of OleT. Specifically, the two sites of decarboxylation, propionates at peripheral tetrapyrrole positions 2 and 4, are positioned such that neither has direct access to the distal pocket where H_2O_2 is activated (Fig. 1). This suggested two possible mechanisms. First, oxidizing equivalents could be conveyed by diffusion of •OH, generated via homolytic cleavage of a ferric hydroperoxy intermediate, from the site of the Fe/H_2O_2 reaction to each propionate. Alternatively, the oxidation could proceed through a relay mechanism involving one or more amino acid side chains as intermediaries, possibly dissecting the requisite hydrogen atom transfer reaction into proton and electron transfer steps.

Results reported here clearly support the latter mechanism. Time-resolved freeze-quench experiments demonstrated the formation and decay of an EPR-active, $S = 1/2$ species during the

course of a single turnover of the decarboxylase–coproheme complex (Fig. 2). This species had power and temperature dependences consistent with its assignment as an organic radical. Narrowing of the spectral line width and loss of ^{1}H-hyperfine coupling in spectra for the D-Tyr–labeled protein allowed assignment of the radical species as a tyrosyl (Fig. S3), which mutagenesis confirmed to be localized specifically at the Tyr-145 side chain (Fig. 3).

Separation between the sites of oxidant activation and substrate oxidation is a recurring motif in metalloenzyme catalysis. Class 1 ribonucleotide reductase provides a classic example, in which oxidizing equivalents are conveyed from the dinuclear iron cluster where O_2 is reductively activated to a nearby tyrosine and ultimately to a catalytic cysteine residue more than 30 Å away (25). Heme-dependent lignin peroxidases translate the oxidizing power of the catalytic Fe(IV)=O (por$^{+\bullet}$) species over similar distances and to the protein surface, allowing the enzyme to access large, water-insoluble lignin substrates (26). A heme/alkylperoxide reaction in prostaglandin synthase generates Fe(IV)=O (por$^{+\bullet}$), which in turn oxidizes a tyrosine side chain to the tyrosyl radical. The tyrosyl specifically abstracts the pro-S hydrogen atom from the C13 position on a large, polyunsaturated arachidonic acid substrate (10). Distinct from OleT, the resulting fatty acyl radical is prevented from transferring an electron to the heme iron; instead, it reacts directly with O_2 to form an intermediate adduct. Heme A synthase and certain cytochrome P450 subtypes are in some ways most analogous to coproheme decarboxylase, because the same heme molecule is both the catalytic moiety and the scaffold for the substrate (3, 4). In each case, oxidation of amino acid side chains by Fe(IV)=O (por+$^{\bullet}$) is proposed to generate amino acid radicals, which, in turn, abstract hydrogen atoms from heme methyl substituents. Subsequent transfer of the resulting electron on the methyl carbon to the heme Fe(IV) generates a methyl carbocation, which is primed for nucleophilic attack by either water or carboxylate side chains.

These examples illustrate how, using one oxidizable amino acid side chain or a series of them, Fe(IV)=O (por$^{+\bullet}$) can extend its reach over sometimes long distances. The amino acid intermediary additionally provides a degree of control over what happens after the initial hydrogen atom abstraction from the substrate. In the case of OleT, in which the hydrogen atom transfers directly to Fe(IV)=O (por$^{+\bullet}$), the resulting substrate radical transfers a second electron to the nearby Fe(IV)=O (por). By contrast, in prostaglandin synthase, the arachidonic acid radical is removed from the analogous Fe(IV)=O (por) species and instead reacts with O_2. Coproheme decarboxylase appears to use Tyr-145 as an intermediary, connecting the oxidizing power of the presumptive Fe(IV)=O (por$^{+\bullet}$) intermediate to the Cβ carbon of each reactive propionate. The resulting propionyl radical electron is then transferred to the Fe(IV).

Although there is no direct evidence as yet for Fe(IV)=O (por$^{+\bullet}$) as the reactive species, the production of Tyr-145$^{\bullet}$ occurred along with loss of the starting ferric coproheme $S = 5/2$ signal and without the clear appearance of new EPR-active species (Fig. 5). These observations are consistent with a mechanism in which ferric coproheme first reacts with H_2O_2 to form a ferric hydroperoxy intermediate. Protonation and heterolytic cleavage of the intermediate would yield Fe(IV)=O (por$^{+\bullet}$) and water. This high-valent species could subsequently remove a hydrogen atom from Tyr-145 to form Tyr-145$^{\bullet}$. In cytochrome P450s or peroxidases with a basic ferryl oxygen, hydrogen atom transfer is expected to deliver an electron to the porphyrin radical cation and a proton to the ferryl in a single, concerted step (27–29). Whereas the destination of the proton from Tyr-145 is not clear, concerted rather than sequential proton and electron transfer from Tyr-145 is attractive, in light of the expected pK_a (~10) and midpoint potential of the neutral tyrosine side chain (30). Hydrogen-bonding contact between propionate 2 and Tyr-145 (Fig. 1) might serve to modulate this pK_a and/or supply a conduit through which the electron is conducted to the macrocycle, as proposed for ascorbate peroxidase and heme model complexes (31, 32). The resulting low-spin d^4 Fe(IV)=O (por) or Fe(IV)–OH (por) species is expected to have integer spin ($S = 1$) and therefore to be EPR-silent (33).

Once formed, Tyr-145$^{\bullet}$ abstracts a hydrogen atom from a nearby propionate Cβ–H in a step that appears to be partially rate-limiting (Fig. 4). Supporting this conclusion, deuteration of the propionate β-carbons elicits a 2-fold (rather than the theoretically predicted 7-fold) decrease in the second-order rate constant for the decarboxylase/H_2O_2 reaction (22). Moreover, about twice as much Tyr-145$^{\bullet}$ accumulates in the time-resolved EPR spectra when the propionate is deuterated, suggesting that this species directly abstracts the hydrogen atom from propionate 2. Hydrogen atom transfer is expected to leave behind a Cβ radical, which we anticipate quickly transfers to the substrate Fe(IV) as CO_2 is lost and a new C=C double bond forms (Scheme 2).

Prior work showed that the initial decarboxylation of propionate 2, yielding harderoheme, is slightly slower than the subsequent decarboxylation of propionate 4. Whereas we inferred that the harderoheme reacted with a second molecule of H_2O_2 to form heme *b*, it was not certain whether this reaction utilized the same Tyr-145 radical. To address this question directly, we generated the decarboxylase–harderoheme complex and monitored its reaction with H_2O_2 by time-resolved, freeze-quench EPR. An $S = 1/2$ signal having line width and hyperfine features similar to those of the analogous coproheme intermediate was observed (Fig. 6). This suggested that harderoheme's propionate 4 is also decarboxylated using Tyr-145$^{\bullet}$ as an intermediary. Whether the harderoheme reacts in the same orientation as shown in Fig. 1 or whether the propionate first forms a hydrogen bonding interaction with Tyr-145, either by leaving the active site and rebinding in a reactive configuration or by rotating ~90° *in situ*, is unknown.

Conclusions

Our results support a catalytic model in which the decarboxylase–coproheme complex reacts with H_2O_2 to form an activated intermediate, possibly Fe(IV)=O (por$^{+\bullet}$), that in turn oxidizes Tyr-145 to Tyr-145$^{\bullet}$. The tyrosyl radical then abstracts a hydrogen atom from the Cβ of propionate 2 in a step that partially limits the overall reaction rate. Electron transfer from the Cβ to Fe(IV) occurs with loss of CO_2 and formation of a new vinyl group. A second round of reaction with H_2O_2 generates Tyr-145$^{\bullet}$ again in the harderoheme complex, allowing for a sec-

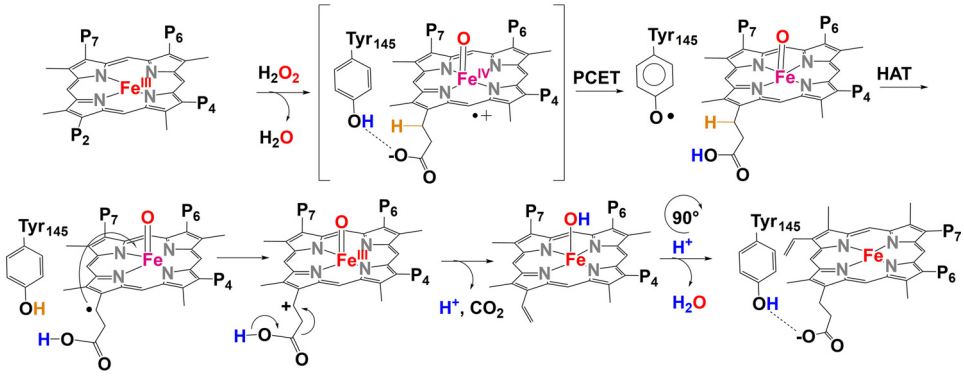

SCHEME 2. Proposed mechanism for coproheme decarboxylation. The Cβ-carbon from which a hydrogen atom is transferred is *labeled*. There is no direct evidence for the intermediacy of a coproheme compound I (shown in *brackets*) or the subsequent Cβ-carbocation species; their presence is merely proposed hypothetically.

ond decarboxylation in turn. This model is reminiscent of mechanisms proposed for heme A synthase or certain cytochrome P450s, both of which undergo oxidative modifications of their methyl side chains or the initial hydrogen atom transfer from arachidonic acid in prostaglandin synthase. The use of tyrosyl radicals as intermediaries in each case allows for a high degree of reaction control and access of the oxidizing species to otherwise hard-to-reach substrates.

Experimental procedures

Preparation of the decarboxylase (HemQ) from S. aureus

Expression and purification of WT and mutant proteins (plasmids available from prior work) were carried out as reported previously (7, 9).

Preparation of the decarboxylase with deuterated tyrosine side chains

L-tyrosine with deuterium substituted for protium at all of its carbon atoms (D_6-L-Tyr, 98% label incorporation) was obtained from Cambridge Isotopes. The decarboxylase was overexpressed in a tyrosine-auxotrophic strain of *Escherichia coli* C43 (DE3) ML14 (Δ*tyrA*) (Addgene) (34), which had been transfected with the same pET28a-*hemQ* construct used above. M63 minimal growth medium contained 3 g/liter KH_2PO_4, 7 g/liter K_2HPO_4, 2 g/liter glucose, 2 g/liter NH_4Cl, 10 mg/liter thiamine, 50 mg/liter kanamycin, 10 μM $CuSO_4$, 30 μM $FeSO_4$, and 1 mM $MgSO_4$). Before inoculation, the medium was supplemented with an amino acid mixture containing 16 mg/liter His, 35 mg/liter Val, 35 mg/liter Phe, 40 mg/liter Leu, 40 mg/liter Asp, 40 mg/liter Ile, and either 80 mg of unlabeled Tyr or 50 mg of D_6-Tyr (L-enantiomers used for all amino acids). A starter culture was generated by inoculating 2 ml of lysogeny broth plus 50 mg/liter kanamycin with a single colony of the expression strain from a freshly streaked plate. The culture was grown on a 250 rpm shaker incubator for 10 h at 37 °C and then used to inoculate (1:500) 10 ml of fresh M63 + amino acids + kanamycin. After 12 h (37 °C, 250 rpm), the 10-ml culture was used to inoculate (1:1000) 6 1-liter flasks of M63 + amino acids + kanamycin. Cultures were grown at 37 °C until an A_{600} of 0.4 was reached. Protein expression was induced by adding isopropyl β-D-1-thiogalactopyranoside (0.5 mM final concentration), and the temperature was lowered to 20 °C. Cells were harvested by centrifugation after 16 h, and the enzyme was purified and substrate was loaded in the same fashion as for the unlabeled enzyme.

Generation of decarboxylase–substrate complexes

Purified protein was incubated at 4 °C in the dark with gentle stirring for 24 h with either the substrate ferric coproheme III, the three-propionate–substituted intermediate (ferric 2-vinyl-4,6,7-tripropionic acid heme, commonly named harderoheme isomer III (35), although it is now understood not to be associated with the harderian gland (36)), or deuterated coproheme III (D-coproheme, synthesis described below) in a 1:1 subunit/coproheme ratio. Unbound coproheme was removed by repeated rounds of centrifuge filtration, and the protein–ligand complexes were further purified on an S-200 Sephacryl gel filtration column (0.4 ml/min). Fractions were collected using an AKTA purification system and then screened via UV-visible spectroscopy (Cary50) for the presence of a ferric porphyrin. Fractions with *Rz* values $\geq$ 0.8 (Rz = absorbance$_{Soret}$/absorbance$_{280\ nm}$) were pooled. For D_6-Tyr–labeled protein, protein with $Rz \geq 0.4$ was retained. Bound porphyrin concentrations were determined by the pyridine hemochrome method. Briefly, 50 μl of protein solution (at 50–300 μM) was mixed with 200 μl of 50 mM NaOH containing 20% pyridine by volume. 3 μl of 0.1 M $K_3(Fe(CN)_6)$ was added, and the oxidized spectrum was measured; 3–5 mg of solid sodium dithionite ($Na_2S_2O_4$) was then added to yield spectra for the reduced pyridine-bound hemes. Difference spectra (reduced minus oxidized, $r - o$) were used to determine the concentration of metalloporphyrin released from the protein. For coproheme, ϵ_{r-o} 546 nm = 23.2 mM^{-1} cm^{-1}; for heme *b*, ϵ_{r-o} 556 nm = 28.4 mM^{-1} cm^{-1}. The Bradford and pyridine hemochrome assays for protein and Fe-porphyrin, respectively, were used to determine the cofactor occupancy in the purified complexes.

Biosynthesis, purification, and characterization of deuterium-labeled coproheme

Site-specifically deuterated coproheme III was synthesized enzymatically *in vitro* (11). The heme biosynthesis enzymes porphobilinogen synthase (HemB), porphobilinogen deaminase (HemC), uroporphyrinogen III synthase (HemD), uroporphyrinogen III decarboxylase (HemE), coproporphyrinogen

oxidase (HemY), and ferrochelatase (HemH) were recombinantly expressed in His_6-tagged forms from synthetic genes in pET 15b or 28a vectors (Genscript). Sequences for the genes encoding HemB, -C, -D, and -E were obtained from the *E. coli* K12 genome in the NCBI database and used without modification (genome accession number NC_000913.3 at location 388753–389727, 3989825–3990766, 3989088–3989828, and 4197716–4198780 for *hemB*, *-C*, *-D*, and *-E*, respectively). Sequences encoding HemY and HemH in *S. aureus* Newman were likewise obtained from NCBI (accession number NC_009641.1 at 1923252–1924652 for *hemY* and 1924676–1925599 for *hemH*) and codon-optimized for heterologous expression in *E. coli*. Individual plasmids were transformed into Tuner(DE3) cells (Novagen). Heterologous expression was carried out in 1-liter flasks of Terrific Broth supplemented with the appropriate antibiotic (kanamycin or ampicillin). Flasks were inoculated 1:100 with a freshly saturated starter culture and grown at 37 °C until an optical density of 0.4–0.6 at 600 nm was reached. Isopropyl β-D-1-thiogalactopyranoside was added to a final concentration of 100 μM, the temperature was lowered to 20 °C, and the cells were grown overnight. Cell pellets harvested by centrifugation were lysed by sonication in buffer A (50 mM Tris, pH 8, 150 mM NaCl, 5 mM imidazole), the lysates were clarified by centrifugation at 45,000 × *g* for 1 h, and the supernatants were loaded onto a nickel-nitrilotriacetic acid affinity column (Bio-Rad) equilibrated with buffer A. Protein was eluted by a 300-ml linear gradient from 0 to 100% buffer B (50 mM Tris, pH 8, 150 mM NaCl, 500 mM imidazole) at 2 ml/min (Akta Prime). The proteins eluted around 40–60% buffer B. Pure fractions were identified via SDS-PAGE, concentrated, dialyzed into 50 mM Tris (pH 8, 150 mM NaCl, with 20% glycerol for HemD), and stored at −80 °C.

Custom-synthesized D_4-ALA (Shanghai Artis Company) was used as the labeled starting material to produce [5, 10, 15, 20, 21, 22, 23, 24-$^2H_{12}$]coproporphyrin III (D-coproporphyrin), in which the carbons β to the propionate carboxylate groups as well as the tetrapyrrole-bridging *meso* carbons are perdeuterated (Scheme 2). Zinc acetate (10 μM), $MgSO_4$ (10 μM), aminolevulinic acid, or D_4-ALA (1 mM), DTT (3 mM), and the four enzymes HemB/C/D/E (2 μM) were degassed by repeated cycles of evacuation and argon back-filling on a Schlenk line and then brought into an anaerobic chamber (Coy). Reactants were combined in 50 ml of 50 mM Tris, pH 8, and stirred overnight in the dark at ambient temperatures (expected theoretical yield, 6.25 μmol of coproporphyrin). After ~16 h, the reactions were removed from the anaerobic chamber and exposed to O_2 from ambient air, and HemY (350 nM) was added. Reactions were stirred at 37 °C in the dark for 1–2 h to fully oxidize the D-coproporphyrinogen to D-coproporphyrin.

The D-coproporphyrin–containing reactions were degassed by repeated cycles of evacuation and N_2 back-filling on a Schlenk line and brought into the anaerobic chamber. HemH (10 μM), DTT (1 mM), and 1.1 eq of ferrous ammonium sulfate were added. After 30 min, the red D-coproheme was removed from the chamber and analyzed by HPLC and MS. For final purification, the D-coproheme–containing reaction was loaded onto two 25-ml C18 solid-phase extraction columns (Restec product no. 26034). The columns were washed with several volumes of H_2O and eluted with methanol, followed by acetonitrile with 0.1% trifluoroacetic acid (TFA) and finally methanol. Each column elution step was dried under N_2, reconstituted in DMSO, and analyzed (see below) before combining and storing the pure fractions at −80 °C. Biosynthetically generated hemes and their precursors were analyzed by the methods outlined below.

HPLC

20–25 μl of porphyrin or heme samples were injected onto a Hypersil Gold PFP 5-μm column (150 × 4.6 mm, Thermo Fisher) attached to an Agillent1100 series HPLC instrument. Solvent A was H_2O with 0.1% TFA, and solvent B was acetonitrile with 0.1% TFA. Samples were run at a flow rate of 2.5 ml/min starting with isocratic 10% B for 3 min, followed by a linear gradient from 10% B to 95% B over 13 min. This was followed by isocratic 95% B for 3 min and a 2-min wash with 10% B. UV-visible absorbance was monitored at 400 nm. Coproporphyrin and coproheme samples were quantified via standard curves (0–20 μM) based on HPLC peak integration.

MS

Tetrapyrrole intermediates and products were analyzed via HPLC in line with electrospray ionization MS to verify their expected masses and deuterium incorporation. HPLC was carried out using an Agilent 1290 system and Agilent PLRP-S PSDVB column (3.0-μm particles, 50 mm × 1.0-mm diameter, P/N PL1312-1300). The column was maintained at 50 °C with a flow rate of 0.6 ml/min. Solvent A consisted of water with 0.1% (v/v) formic acid. Solvent B was acetonitrile with 0.1% formic acid. The column was equilibrated to 5% B before sample injection. A linear gradient from 5 to 95% B was used from 1.0 to 4.0 min, followed by 95% B (4.0–5.0 min) and 5% B (5.0–6.0 min). Column eluate was imported into an Agilent 6538 quadrupole time of flight (QTOF) mass spectrometer with an electrospray ionization source. Source parameters were as follows: drying gas, 8.0 liters/min; drying gas heat, 350 °C; nebulizer 55 p.s.i.; capillary voltage, 3500 V; capillary exit, 100 V. Spectra were collected in positive mode from 50 to 1700 *m*/*z* at a rate of 2 Hz.

NMR spectroscopy

Coproporphyrin III, D-coproporphyrin III, and their aminolevulinic acid precursors were analyzed by NMR to assess the position and extent of deuterium label incorporation into the latter. All compounds were characterized by ^1H using a Bruker 300-MHz NMR and/or a Bruker AVANCE III 500-MHz NMR spectrometer, equipped with a Prodigy™ cryoprobe and SampleJet™ automatic sample-loading system. Chemical shifts are reported in ppm (δ) relative to the residual solvent peak in the corresponding spectra (deuterium oxide δ 4.79, D_4-methanol δ 3.31), and coupling constants (*J*) are reported in hertz (Hz) and analyzed using MestReC NMR data processing.

Monitoring decarboxylase reactions in real time with stopped-flow UV-visible spectroscopy

Data were measured using a Hi-Tech Scientific stopped-flow spectrometer in single mixing mode with diode array detection. The decarboxylase–ferric tetrapyrrole complex (5–10 μM) was

rapidly mixed (<1.5 ms) with variable concentrations of H_2O_2/D_2O_2 or peracetic acid before measurement of spectra. Data were measured at varying time points and fit using Kinetic Studio (Hi-Tech Scientific) software to exponential decay functions to determine rate constants (k_{obs}). For each experimental condition, all data were measured in at least triplicate and averaged. Plots of k_{obs} *versus* oxidant concentration were fit with linear least-squares regression analysis to determine second-order rate constants (Kaleidagraph). Reactions were carried out over a range of pH values in either 50 mM potassium phosphate (pH 5.8, 6.6, and 7.4) or 50 mM Tris-Cl (pH 8.2 or 8.8).

Time-resolved EPR spectroscopic analyses of the reaction of decarboxylase–tetrapyrrole complexes with H_2O_2

EPR data were measured on a Bruker EMX EPR spectrometer (X-band, 9.37 MHz) using a Bruker Cold Edge (Sumitomo Cryogenics) cryogen-free system with a Mercury iTC controller unit. In all cases, averages of four scans are reported. For the reaction time course experiments, 120-μl aliquots of enzyme–substrate complex (200 μM, pH/D 8.8, 298 K) were manually mixed inside the EPR tube with an equal volume of H_2O_2 (D_2O_2) containing either 10 or 300 eq of the oxidant and frozen in liquid N_2 at time points between 30 and 300 s. Organic radical spectra were measured at 77 K, 25-μW microwave power, 100-kHz modulation frequency, and 5-G modulation amplitude. Signals were double-integrated over 3250–3450 G (OriginLab) and compared with TEMPO standards (0, 25, 50, and 100 μM) measured under similar conditions for spin quantitation. Iron spectra were measured at 15 K with 2-mW microwave power over a field of 500–3500 G. Spectral g-values were determined via simulations of experimental data sets utilizing Easyspin software (37).

For studies of the dependence of the organic radical EPR signal intensity on temperature, the instrument parameters were the same as above but with temperatures set at intervals between 15 and 200 K. The normalized intensity (I_n) was plotted *versus* temperature.

$$I_n = \frac{(I_o \times T \times 10^{-\frac{dB}{20}})}{\text{gain}} \quad \text{(Eq. 2)}$$

Here, I_o is the doubly integrated signal, T is temperature, dB is microwave power, and gain is the amplifier gain.

For studies of the power saturation properties of the organic radical EPR signal, data were measured over 0.85 μW to 103 mW at 77 K. The power at half-saturation ($P_{½}$) was determined via nonlinear least-squares regression analysis of the $\log(I/P^{0.5})$ *versus* P plots using Equation 3,

$$\log\left(\frac{I}{\sqrt{P}}\right) = -\left(\frac{b}{2}\right)\log(P_{\frac{1}{2}}^{1} + P) + \left(\frac{b}{2}\right)\log(P_{\frac{1}{2}}^{1}) + \log(k) \quad \text{(Eq. 3)}$$

where P is the microwave power, I is the peak-to-trough EPR signal intensity, b is a factor describing the homogeneity of the radical signal (where a value of 1 is non-homogenous and a value of 3 is completely homogenous), and k is an intensity correction factor.

Author contributions—B. R. S., A. I. C., G. C. M., and J. L. D. conceptualization; B. R. S., A. I. C., G. C. M., K. S., and J. L. D. data curation; B. R. S., A. I. C., G. C. M., E. M. S., and J. L. D. formal analysis; B. R. S. and J. L. D. project administration; B. R. S., A. I. C., K. S., K. R. R., G. S. L.-R., and J. L. D. writing-review and editing; K. S. and J. L. D. investigation; K. S. and J. L. D. methodology; E. M. S. software; J. L. D. supervision; J. L. D. funding acquisition; J. L. D. writing-original draft.

References

1. Unno, M., Matsui, T., and Ikeda-Saito, M. (2007) Structure and catalytic mechanism of heme oxygenase. *Nat. Prod. Rep.* **24,** 553–570 CrossRef Medline
2. Wilks, A., and Heinzl, G. (2014) Heme oxygenation and the widening paradigm of heme degradation. *Arch. Biochem. Biophys.* **544,** 87–95 CrossRef Medline
3. Brown, K. R., Brown, B. M., Hoagland, E., Mayne, C. L., and Hegg, E. L. (2004) Heme A synthase does not incorporate molecular oxygen into the formyl group of heme A. *Biochemistry* **43,** 8616–8624 CrossRef Medline
4. Colas, C., and Ortiz de Montellano, P. R. (2003) Autocatalytic radical reactions in physiological prosthetic heme modification. *Chem. Rev.* **103,** 2305–2332 CrossRef Medline
5. Dailey, H. A., Gerdes, S., Dailey, T. A., Burch, J. S., and Phillips, J. D. (2015) Noncanonical coproporphyrin-dependent bacterial heme biosynthesis pathway that does not use protoporphyrin. *Proc. Natl. Acad. Sci. U.S.A.* **112,** 2210–2215 CrossRef Medline
6. Dailey, H. A., Dailey, T. A., Gerdes, S., Jahn, D., Jahn, M., O'Brian, M. R., and Warren, M. J. (2017) Prokaryotic heme biosynthesis: multiple pathways to a common essential product. *Microbiol. Mol. Biol. Rev.* **81,** e00048-16 Medline
7. Celis, A. I., Streit, B. R., Moraski, G. C., Kant, R., Lash, T. D., Lukat-Rodgers, G. S., Rodgers, K. R., and DuBois, J. L. (2015) Unusual peroxide-dependent, heme-transforming reaction catalyzed by HemQ. *Biochemistry* **54,** 4022–4032 CrossRef Medline
8. Streit, B. R., Celis, A. I., Shisler, K., Rodgers, K. R., Lukat-Rodgers, G. S., and DuBois, J. L. (2017) Reactions of ferrous coproheme decarboxylase (HemQ) with O-2 and H_2O_2 yield ferric heme *b*. *Biochemistry* **56,** 189–201 CrossRef Medline
9. Celis, A. I., Gauss, G. H., Streit, B. R., Shisler, K., Moraski, G. C., Rodgers, K. R., Lukat-Rodgers, G. S., Peters, J. W., and DuBois, J. L. (2017) Structure-based mechanism for oxidative decarboxylation reactions mediated by amino acids and heme propionates in coproheme decarboxylase (HemQ). *J. Am. Chem. Soc.* **139,** 1900–1911 CrossRef Medline
10. Tsai, A., Kulmacz, R. J., and Palmer, G. (1995) Spectroscopic evidence for reaction of prostaglandin-H synthase-1 tyrosyl radical with arachidonic acid. *J. Biol. Chem.* **270,** 10503–10508 CrossRef Medline
11. Layer, G., Pierik, A. J., Trost, M., Rigby, S. E., Leech, H. K., Grage, K., Breckau, D., Astner, I., Jänsch, L., Heathcote, P., Warren, M. J., Heinz, D. W., and Jahn, D. (2006) The substrate radical of *Escherichia coli* oxygen-independent coproporphyrinogen III oxidase HemN. *J. Biol. Chem.* **281,** 15727–15734 CrossRef Medline
12. Barry, B. A., el-Deeb, M. K., Sandusky, P. O., and Babcock, G. T. (1990) Tyrosine radicals in photosystem II and related model compounds: characterization by isotopic labeling and EPR spectroscopy. *J. Biol. Chem.* **265,** 20139–20143 Medline
13. Khindaria, A., and Aust, S. (1996) EPR detection and characterization of lignin peroxidase porphyrin pi-cation radical. *Biochemistry* **35,** 13107–13111 CrossRef Medline
14. Fujii, H., Yoshimura, T., and Kamada, H. (1996) ESR studies of A(1u) and A(2u) oxoiron(IV) porphyrin π-cation radical complexes: spin coupling between ferryl iron and A(1u)/A(2u) orbitals. *Inorg. Chem.* **35,** 2373–2377 CrossRef Medline
15. Yeh, H. C., Gerfen, G. J., Wang, J. S., Tsai, A. L., and Wang, L. H. (2009) Characterization of the peroxidase mechanism upon reaction of prostacyclin synthase with peracetic acid: identification of a tyrosyl radical intermediate. *Biochemistry* **48,** 917–928 CrossRef Medline

16. Schünemann, V., Lendzian, F., Jung, C., Contzen, J., Barra, A. L., Sligar, S. G., and Trautwein, A. X. (2004) Tyrosine radical formation in the reaction of wild type and mutant cytochrome P450cam with peroxy acids: a multifrequency EPR study of intermediates on the millisecond time scale. *J. Biol. Chem.* **279,** 10919–10930 CrossRef Medline
17. Di Bilio, A. J., Crane, B. R., Wehbi, W. A., Kiser, C. N., Abu-Omar, M. M., Carlos, R. M., Richards, J. H., Winkler, J. R., and Gray, H. B. (2001) Properties of photogenerated tryptophan and tyrosyl radicals in structurally characterized proteins containing rhenium(I) tricarbonyl diimines. *J. Am. Chem. Soc.* **123,** 3181–3182 CrossRef Medline
18. Bender, C., Sahlin, M., Babcock, G., Barry, B., Chandrashekar, T., Salowe, S., Stubbe, J., Lindstrom B., Petersson, L., Ehrenberg, A., and Sjoberg, B. (1989) An ENDOR study of the tyrosyl free-radical in ribonucleotide reductase from *Escherichia coli*. *J. Am. Chem. Soc.* **111,** 8076–8083 CrossRef
19. Svistunenko, D. A., and Cooper, C. E. (2004) A new method of identifying tyrosyl radicals in proteins. *Biophys. J.* **87**, 582–595 CrossRef Medline
20. Westerlund, K., Berry, B. W., Privett, H. K., and Tommos, C. (2005) Exploring amino-acid radical chemistry: protein engineering and *de novo* design. *Biochim. Biophys. Acta* **1707,** 103–116 CrossRef Medline
21. Roston, D., Islam, Z., and Kohen, A. (2014) Kinetic isotope effects as a probe of hydrogen transfers to and from common enzymatic cofactors. *Arch. Biochem. Biophys.* **544,** 96–104 CrossRef Medline
22. Frey, P. A., and Hegeman, A. D. (2007) *Enzymatic Reaction Mechanisms*, pp. 91–101, Oxford University Press, Oxford, UK
23. Hofbauer, S., Dalla Sega, M., Scheiblbrandner, S., Jandova, Z., Schaffner, I., Mlynek, G., Djinović-Carugo, K., Battistuzzi, G., Furtmüller, P. G., Oostenbrink, C., and Obinger, C. (2016) Chemistry and molecular dynamics simulations of heme *b*-HemQ and coproheme-HemQ. *Biochemistry* **55,** 5398–5412 CrossRef Medline
24. Grant, J. L., Hsieh, C. H., and Makris, T. M. (2015) Decarboxylation of fatty acids to terminal alkenes by cytochrome P450 compound I. *J. Am. Chem. Soc.* **137,** 4940–4943 CrossRef Medline
25. Stubbe, J., Nocera, D. G., Yee, C. S., and Chang, M. C. Y. (2003) Radical initiation in the class I ribonucleotide reductase: long-range proton-coupled electron transfer? *Chem. Rev.* **103,** 2167–2201 CrossRef Medline
26. Doyle, W. A., Blodig, W., Veitch, N. C., Piontek, K., and Smith, A. T. (1998) Two substrate interaction sites in lignin peroxidase revealed by site-directed mutagenesis. *Biochemistry* **37,** 15097–15105 CrossRef Medline
27. Efimov, I., Badyal, S. K., Metcalfe, C. L., Macdonald, I., Gumiero, A., Raven, E. L., and Moody, P. C. (2011) Proton delivery to ferryl heme in a heme peroxidase: enzymatic use of the Grotthuss mechanism. *J. Am. Chem. Soc.* **133,** 15376–15383 CrossRef Medline
28. Rittle, J., and Green, M. T. (2010) Cytochrome P450 compound I: capture, characterization, and C–H bond activation kinetics. *Science* **330,** 933–937 CrossRef Medline
29. Gumiero, A., Metcalfe, C. L., Pearson, A. R., Raven, E. L., and Moody, P. C. (2011) Nature of the ferryl heme in compounds I and II. *J. Biol. Chem.* **286,** 1260–1268 CrossRef Medline
30. Warren, J. J., Tronic, T. A., and Mayer, J. M. (2010) Thermochemistry of proton-coupled electron transfer reagents and its implications. *Chem. Rev.* **110,** 6961–7001 CrossRef Medline
31. Macdonald, I. K., Badyal, S. K., Ghamsari, L., Moody, P. C., and Raven, E. L. (2006) Interaction of ascorbate peroxidase with substrates: a mechanistic and structural analysis. *Biochemistry* **45,** 7808–7817 CrossRef Medline
32. Warren, J. J., and Mayer, J. M. (2011) Proton-coupled electron transfer reactions at a heme-propionate in an iron-protoporphyrin-IX model compound. *J. Am. Chem. Soc.* **133,** 8544–8551 CrossRef Medline
33. Schulz, C. E., Devaney, P. W., Winkler, H., Debrunner, P. G., Doan, N., Chiang, R., Rutter, R., and Hager, L. P. (1979) Horseradish peroxidase compound I: evidence for spin coupling between the heme iron and a "free" radical. *FEBS Lett.* **103,** 102–105 CrossRef Medline
34. Lin, M. T., Sperling, L. J., Frericks Schmidt, H. L., Tang, M., Samoilova, R. I., Kumasaka, T., Iwasaki, T., Dikanov, S. A., Rienstra, C. M., and Gennis, R. B. (2011) A rapid and robust method for selective isotope labeling of proteins. *Methods* **55,** 370–378 CrossRef Medline
35. Lash, T. D., Mani, U. N., Keck, A. A., and Jones, M. A. (2010) Normal and abnormal heme biosynthesis. 6. Synthesis and metabolism of a series of monovinylporphyrinogens related to harderoporphyrinogen: further insights into the oxidative decarboxylation of porphyrinogen substrates by coproporphyrinogen oxidase. *J. Org. Chem.* **75,** 3183–3192 CrossRef Medline
36. Gorchein, A., Danton, M., and Lim, C. K. (2005) Harderoporphyrin: a misnomer. *Biomed. Chromatogr.* **19,** 565–569 CrossRef Medline
37. Stoll, S., and Schweiger, A. (2006) EasySpin, a comprehensive software package for spectral simulation and analysis in EPR. *J. Magn. Reson.* **178,** 42–55 CrossRef Medline

Decarboxylation involving a ferryl, propionate, and a tyrosyl group in a radical relay yields heme *b*

Bennett R. Streit, Arianna I. Celis, Garrett C. Moraski, Krista A. Shisler, Eric M. Shepard, Kenton R. Rodgers, Gudrun S. Lukat-Rodgers and Jennifer L. DuBois

J. Biol. Chem. 2018, 293:3989-3999.
doi: 10.1074/jbc.RA117.000830 originally published online February 2, 2018